Inorganic Chemistry

Article

pubs.acs.org/IC

Heterometallic $Co^{III}_4Fe^{III}_2$ Schiff Base Complex: Structure, Electron Paramagnetic Resonance, and Alkane Oxidation Catalytic Activity

Dmytro S. Nesterov,[†] Eduard N. Chygorin,[‡] Volodymyr N. Kokozay,*[,‡] Volodymyr V. Bon,[§] Roman Boča,[∥,⊥] Yuriy N. Kozlov,[⊗] Lidia S. Shul'pina,[○] Julia Jezierska,[#] Andrew Ozarowski,[▽] Armando J. L. Pombeiro,*[,†] and Georgiy B. Shul'pin[⊗]

[†]Centro de Química Estrutural, Complexo I, Instituto Superior Técnico, Technical University of Lisbon, Av. Rovisco Pais, 1049-001, Lisbon, Portugal

[‡]Department of Inorganic Chemistry, Taras Shevchenko National University of Kyiv, 64 Volodymyrska St., 01601 Kyiv, Ukraine

[§]Department of Chemistry of Complex Compounds, V. I. Vernadsky Institute of General and Inorganic Chemistry, National Academy of Sciences of Ukraine, 32/34 Palladin Ave., Kyiv 03680, Ukraine

[∥]Institute of Inorganic Chemistry, FCHPT, Slovak University of Technology, Radlinskeho 9, 812 37 Bratislava, Slovakia

[⊥]Department of Chemistry, FPV, University of SS Cyril and Methodius, Trnava, Slovakia

[⊗]Semenov Institute of Chemical Physics, Russian Academy of Sciences, Ulitsa Kosygina, dom 4, Moscow 119991, Russia

[○]Nesmeyanov Institute of Organoelement Compounds, Russian Academy of Sciences, Ulitsa Vavilova, dom 28, Moscow 119991, Russia

[#]Faculty of Chemistry, University of Wroclaw, 14 Joliot-Curie Str., 50-383, Wroclaw, Poland

[▽]National High Magnetic Field Laboratory, Florida State University, 1800 E. Paul Dirac Drive, Tallahassee, Florida 32310, United States

Supporting Information

ABSTRACT: The heterometallic complex $[Co_4Fe_2OSae_8]\cdot 4DMF\cdot H_2O$ (**1**) was synthesized by one-pot reaction of cobalt powder with iron chloride in a dimethylformamide solution of salicylidene-2-ethanolamine (H_2Sae) and characterized by single crystal X-ray diffraction analysis, magnetic measurements, high frequency electron paramagnetic resonance (HF-EPR), and Mössbauer spectroscopies. The exchange coupling in the Fe(III)−Fe(III) pair is of antiferromagnetic behavior with $J/hc = -190$ cm^{-1}. The HF-EPR spectra reveal an unusual pattern with a hardly detectable triplet signal of the Fe(III) dimer. The magnitude of D (ca. 13.9 cm^{-1}) was found to be much larger than in related dimers. The catalytic investigations disclosed an outstanding activity of **1** toward oxidation of cycloalkanes with hydrogen peroxide, under mild conditions. The most efficient system showed a turnover number (TON) of 3.57×10^3 with the concomitant overall yield of 26% for cyclohexane, and 2.28×10^3/46%, respectively, for cyclooctane. A remarkable turnover frequency (TOF) of 1.12×10^4 h^{-1} (the highest initial rate $W_0 = 3.5 \times 10^{-4}$ M s^{-1}) was achieved in oxidation of cyclohexane. Kinetic experiments and selectivity parameters led to the conclusion that hydroxyl radicals are active (attacking C−H bonds) species. Kinetic and electrospray ionization mass spectrometry (ESI-MS) data allowed us to assume that the trinuclear heterometallic particle $[Co_2Fe(Sae)_4]^+$, originated from **1** in solution, could be responsible for efficient generation of hydroxyl radicals from hydrogen peroxide.

INTRODUCTION

The ongoing interest in heterometallic transition metal complexes arises from their diverse applications.[1] Many studies in this area have been stimulated by the magnetic properties of these materials.[2] However, one of the most common application fields for coordination compounds—catalysis—is still practically unexplored in the case of heterometallic transition metal complexes with classical N,O-donor ligands, in contrast to organometallic ones.[3] On the other hand, the biological metalloenzymes, which represent a peak of perfection in the art of catalysis, often contain heterometallic active sites,[4] thus suggesting the advantage in utilizing heterometallic catalytic systems.

Some of us have recently demonstrated that heterobi- and heterotrimetallic coordination compounds of $Cu^{II}/Co^{III}/Fe^{III}$ and $Cu^{II}/Co^{III}/Co^{II}_2$ metal compositions with aminoalcohols can act as remarkably active and selective catalysts for oxidation of alkanes with H_2O_2 under mild conditions.[5,6] These results can be associated with the synergic effect of few different metals and, particularly, the outstanding activity of the Cu/Co/Fe

Received: July 6, 2012
Published: August 1, 2012

   dx.doi.org/10.1021/ic301460q | Inorg. Chem. 2012, 51, 9110−9122

complex could point to the crucial role of iron. It was also shown that the presence of Ni^{II} or Zn^{II} ions instead of Fe^{III} or Co^{II}, respectively,[5,6] had a strong inhibitory effect on the catalytic activity, probably because of inability of Zn^{II} and limited ability of Ni^{II} to participate in oxidation chemistry under the employed conditions.

On the basis of these considerations, we focused our studies on the search for polynuclear heterometallic M/Fe complexes exhibiting oxidation catalytic activity. The "direct synthesis" (DS) proved to be a powerful strategy for the self-assembly preparation of polynuclear complexes possessing unprecedented structures,[5,7] and it was chosen as the main synthetic approach in the present investigation. The flexible, polydentate N,O-donor Schiff base salicylidene-2-ethanolamine (H_2Sae) was chosen because of its recognized ability to generate sophisticated coordination assemblies under spontaneous self-assembly conditions.[8] The usage of DS with this ligand, prepared in situ, resulted in a hexanuclear heterometallic complex $[Co_4Fe_2OSae_8]\cdot 4DMF\cdot H_2O$ (**1**), whose unique structure, magnetic properties, uncommon electron paramagnetic resonance (EPR) spectra, and unprecedented catalytic activity are discussed here.

RESULTS AND DISCUSSION

Synthesis of 1. The Schiff base H_2Sae was prepared in situ as described,[8c] by condensation of salicylaldehyde with ethanolamine in dimethylformamide (DMF) prior to addition of other reagents. The one-pot reaction of cobalt powder and $FeCl_2\cdot 4H_2O$ with this solution in open air gave a red mixture, out of which dark brown crystals of **1** precipitated after one day. The formation of **1** (solvate DMF and water molecules are not shown) can be accounted for by the following overall reaction scheme:

$$4Co^0 + 2FeCl_2 + 8H_2Sae + 4Et_3N + 3.5O_2 \rightarrow [Co_4Fe_2OSae_8] + 4Et_3N\cdot HCl + 6H_2O$$

The in situ formation of Schiff base at the first stage (before addition of the metals) was confirmed by ^1H NMR spectrum (in $DMSO/CCl_4$) of the oil formed by evaporation of solvent, where the singlet at 8.39 ppm corresponds to the characteristic −CH═N−proton (Supporting Information, Figure S1).[9] The usage of the initial reagents in stoichiometric ratios gives a constant yield and reproducibility of the synthesis. Other molar ratios (for example Co: $FeCl_2$: H_2Sae =1: 1: 1) can also be used for the preparation of **1**, but with lower yield and longer crystallization time. The details of IR spectra of **1** as well as the thermogravimetric studies are described in the Supporting Information.

Crystal Structure. The structure of **1** features a hexanuclear array composed of two trinuclear $\{Co_2Fe(Sae)_4\}$ fragments linked by a single oxygen atom (Figures 1, Supporting Information, Figure S4; Table S2). The cobalt atom adopts an almost regular octahedral geometry, being coordinated by two aminoalcohol ligands with the Co−O(N) distances varying from 1.872(3) to 1.934(3) Å. Such N_2O_4 coordination environment is typical for cobalt in a trivalent oxidation state. The coordination polyhedra around the iron atoms can be described as a compressed square pyramid with the Fe−O axial bond lengths of 1.7837(7) and 1.7799(10) Å for two crystallographically independent units.

The combination of four octahedra with two square pyramids (Figure 1) results in a $M_6(\mu\text{-}X)_9$ molecular structure

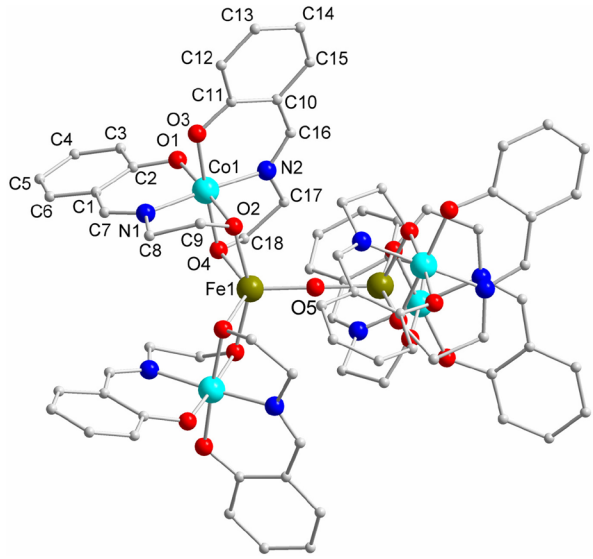

Figure 1. Molecular structure of **1** with the atom numberings (hydrogen atoms from were omitted for clarity). Color codes: Co, cyan; Fe, brown.

type (MST, X means oxygen for the case of **1**), which, as will be demonstrated below, represents the most prominent structural feature of **1** (Figure 2). As we showed before, according to the

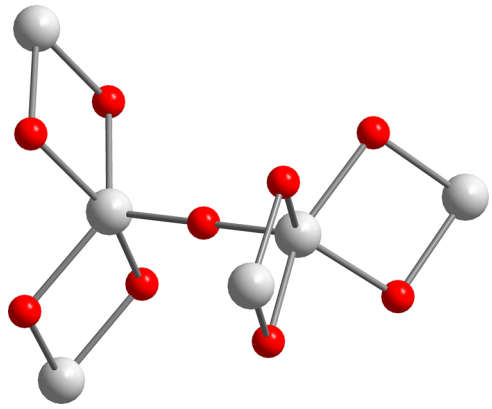

Figure 2. Ball-and-stick representation of the $M_6(\mu\text{-}X)_9$ MST in **1**.

Cambridge Structural Database (CSD),[10] the number of hexanuclear complexes ranks in the fourth place (ca. 1300 hits) among all other polynuclear coordination compounds with $M(\mu\text{-}X)_nM$ (n = 1−4) bridging between metal centers.[11] Six metal centers can be combined in various manners and, in contrast to tetra- or pentanuclear MSTs,[6,11] the speculative evaluation of all possible M_6X_b combinations becomes difficult because of their great diversity: a careful analysis for this case should be based on "reciprocal" strategy, generating possible M_6X_b combinations followed by searches via CSD. General observations suggest that the metal centers and bridging atoms tend to pack as compact as possible and to form symmetric M_aX_b assemblies.

Although one can select a few most symmetric MSTs, where six metal centers form a line (Figure 3), rod, or wheel, these types cover only about 20% of all the hexanuclear structures (the wheel type is the leading one with 105 hits). Most of the others have distorted or unclear MSTs, which can be hardly classified. The structure of **1** is also highly symmetric, belonging

dx.doi.org/10.1021/ic301460q | Inorg. Chem. 2012, 51, 9110−9122

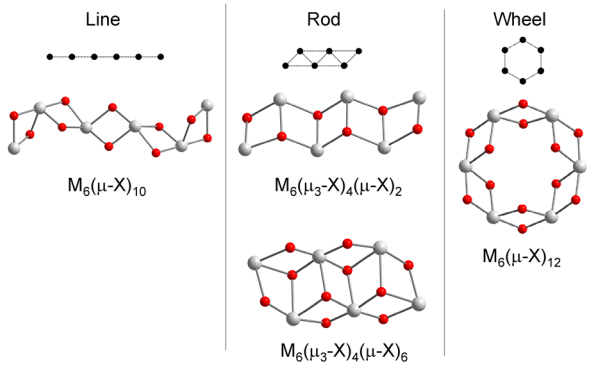

Figure 3. Some typical interconnections between metal centers for the case of hexanuclear complexes and the respective MSTs.

to the S_4 point group. The linkage by one oxygen atom results in a quite rare MST $M_6(\mu\text{-X})_9$ and, as far as we are aware of, the only known compound possessing such a structure is the heterometallic complex $[Cd_2Cl\{Co(aet)_2(en)_2\}](NO_3)_7$ (**2**) (aet = 2-aminoethanethiolate; en = ethylenediamine),[12] the structure of which is depicted at Figure 4. Although the

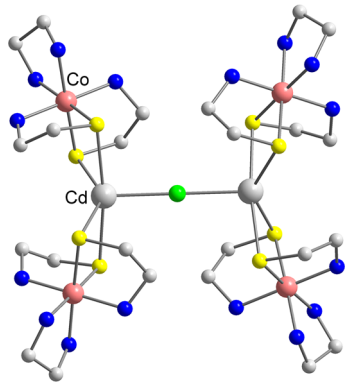

Figure 4. Molecular structure of the complex $[Cd_2Cl\{Co(aet)_2(en)_2\}](NO_3)_7$,[25] showing the same MST as for **1**.

topologies of the $M_6(\mu\text{-X})_9$ cores in **1** and **2** are equal, the geometric configurations are different: the planes formed by Co_2Fe triangles in **1** are perpendicular (Figure 2), while in **2** the respective Co_2Cd trinuclear fragments lie approximately in one plane (torsion angle Co···Cd···Cd′···Co′ is 23.7°). The obvious reason for the distortion of the structure of **1** is the sterical hindrance of the bulky Sae ligands.

The MST of **1** and **2** is quite rare, and the M(μ-X)M bridge seems to be the most important feature. Particularly, the initial search within the CSD toward the hexanuclear coordination compounds containing such a type of bridging, at least one M(μ-X)M bridge, gave only 35 hits, and most of them had a cyclic structure (Figure 5). In the search for polynuclear compounds where two M_aX_b arrays would be connected just by one bridging atom we extended our search to a broader range of nuclearities (four and more metal centers were included). To our great surprise, the new search did not reveal a great number of desired compounds (153 hits were selected). Approximately a half of the structures that formally fit the search conditions were found to be based on the same $M_4(\mu\text{-X})_6$ and $M_4(\mu\text{-X})_4$ tetranuclear MSTs (Figure 5), 25 and 55 hits, respectively. Finally, careful examination of the results revealed only 13 compounds (see ESI for refcode list) of the type M_aX_b–X–

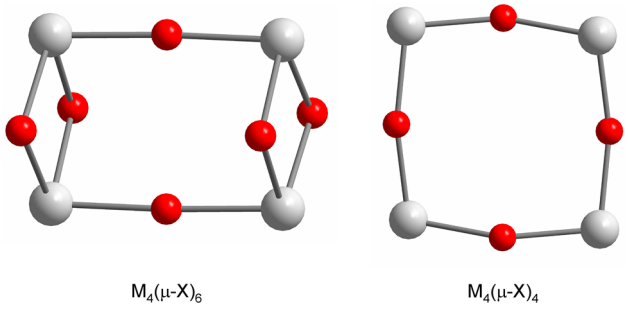

Figure 5. Most typical MSTs (among all structures in CSD), possessing M(μ-X)M bridge.

M_cX_d (MST of **1** can be written as M_2X_4–X–M_2X_4), evidencing that a single M(μ-X)M bridge between two polynuclear M_aX_b fragments is quite rare.

The question arising in this context is that how is such an uncommon structure, as that of **1**, formed. To answer this, one can propose the general formation scheme (Figure 6). The

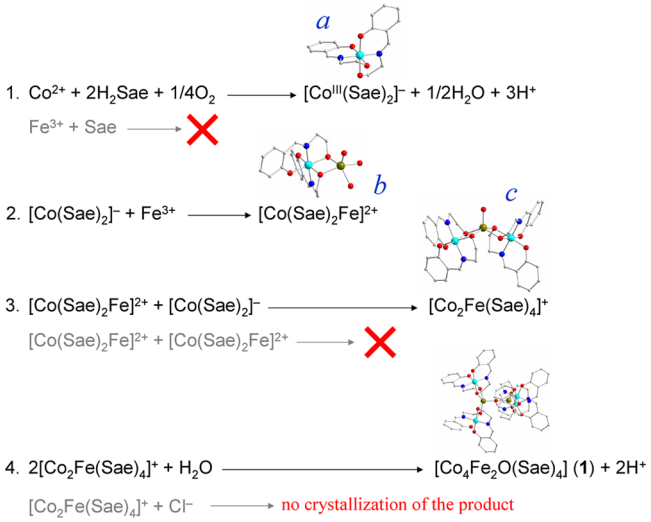

Figure 6. Proposed formation of **1**. Side reactions are marked by gray.

coordination mode of the Schiff base ligand to a Co center leads to the formation of a *mer*-$[Co^{III}(HSae)(Sae)]$ unit (*a*) with the octahedral environment N_2O_4 typical for cobalt(III), while the participation of iron(III) in such a reaction is less probable. At the next stage, free iron ion is coordinated to form a binuclear $[CoFe(Sae)_2]^{2+}$ block (*b*), where the free sites in the coordination environment of iron are occupied by solvent molecules and chloride anions.

Although the reaction of two blocks *b* could lead to a tetranuclear Co_2Fe_2 fragment, the excess of cobalt ions in the reaction mixture forces the interaction of the cobalt unit *a* with the binuclear unit *b*, resulting in a trinuclear block *c* $[Co_2Fe(Sae)_4]^+$. The coordination of a third block *a* with the formation of a Co_3Fe fragment is unlikely because of the sterical hindrance of bulky benzene rings of the ligand. Finally, two blocks *c* form a hexanuclear structure of **1** through the Fe–O–Fe oxo-bridge. In contrast to previous steps, the last one is most difficult to explain: why does compound *c* not crystallize as a trinuclear $[Co_2Fe(Sae)_4]Cl$ complex, but forms a dimer? First, looking at the dimeric structure (Figure 7) one can notice a self-complementary nature of the trinuclear fragments, rotated

dx.doi.org/10.1021/ic301460q | Inorg. Chem. 2012, 51, 9110–9122

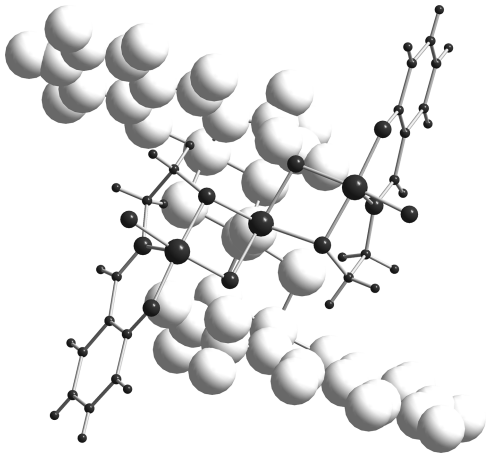

Figure 7. Illustration of the conformity between two trinuclear $\{Co_2Fe(Sae)_4\}$ fragments (black and white), rotated to 90°, forming the hexanuclear molecule of **1**. A view along Fe−O−Fe line; only one pair of Sae ligands are shown.

90° to each other, where the dimer is strengthened by weak C−H···O and van der Waals interactions.

However, the compound **2** possessing the same MST (Figure 4) does not exhibit such intramolecular interactions,[12] pointing to their secondary role. The synthetic scheme of **2** includes the elimination of excess chloride anion from the reaction mixture, leading to a polynuclear structure. Analogously, the presence of Et_3N in the reaction mixture of **1** leads to the formation of the salt $Et_3N{\cdot}HCl$ (see reaction scheme), promoting the main reaction (step 4 in Figure 6), while the side reaction of step 4 is suppressed. To confirm this, we attempted to prepare complex **1** without using a base (a key component), and the desired product was not obtained.

Magnetic Measurements. The effective magnetic moment for complex **1** at T = 300 K is μ_{eff} = 2.97 μ_B and on cooling it gradually decreases to μ_{eff} = 1.10 μ_B at T = 50 K. Below this temperature its decrease is less gradual to μ_{eff} = 0.95 μ_B at T = 7 K and then the effective magnetic moment drops down more rapidly (Figure 8).

The stoichiometry of the complex **1** shows the presence of two Fe(III) centers linked by a nearly linear oxido-bridge. The peripheral cobalt(III) atoms of the whole H-type architecture

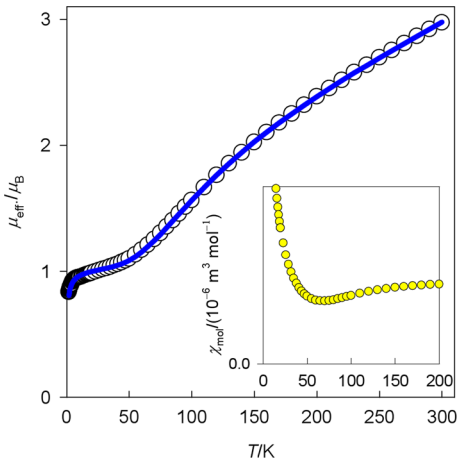

Figure 8. Temperature dependence of the effective magnetic moment for **1**. Open circles, experimental data; solid line, fitted.

are magnetically silent. This implies that a model of the exchange coupled Fe(III) pair could be appropriate

$$\hat{H}^{iso} = -J(\vec{S}_A \cdot \vec{S}_B)\hbar^{-2} + \mu_B g_{iso} B(\hat{S}_{Az} + \hat{S}_{Bz})\hbar^{-1}$$

In the case of antiferromagnetic exchange, the ground state is S = 0 and the excited spin multiplets are S = 1, 2, 3, 4, and 5 when the spin state of the Fe atoms is S = 5/2. A very steep decrease of the effective magnetic moment suggests that J is very negative. In such a case the excited triplet state is well separated from the ground state singlet. The high-temperature limit for the effective magnetic moment of a system of two metal ions is $\mu_{eff}/\mu_B = g_{iso}[2s(s+1)]^{1/2}$ which amounts to μ_{eff}/μ_B = 4.18 g_{iso} for S = 5/2.

Inclusion of the single-ion zero-field splitting into the model offers no improvement because its effects can only be significant at very low temperatures at which S = 1 and higher states of the dimer are not populated. The S = 0 ground state implies that the magnetic susceptibility should vanish for T approaching zero. Inspection to Figure 8 shows that this is not the case, as the vanishing susceptibility signal from the diad is replaced by the rising susceptibility of a paramagnetic impurity at low temperatures. Therefore the susceptibility has been fitted by using

$$\chi_{sample} = (1 - x_{PI})\chi_{diad} + 2x_{PI}C_{PI}/(T - \Theta_{PI}) + \alpha$$

where the Curie constant $C_{PI} = (N_A\mu_0\mu_B^2/k_B)g_{PI}^2 S_{PI}(S_{PI} + 1)/3$ contains the basic physical constants in their usual meaning; g_{PI} = 2 and S_{PI} = 5/2 have been assumed.

The fitting procedure yielded the following set of magnetic parameters: J/hc = −190 cm^{-1}, g_{iso} = 2.008, the temperature-independent term α = 2.5 × 10^{-9} m^3 mol^{-1}, the mole fraction of the paramagnetic impurity x_{PI} = 0.014, and the Weiss constant for the PI is Θ_{PI} = −0.88 K. The quality of the fit is very good: the discrepancy factor $R(\chi)$ = 0.015 (Figure 8).

Mössbauer Spectroscopy. One quadrupole doublet was seen in the Mössbauer spectra (Figure 9). The small isomer shift IS = 0.335(1) (versus α-iron) and small quadrupole splitting QS = 0.692(6) are consistent with the $^6A_1$ state of the iron(III) ions in **1**.

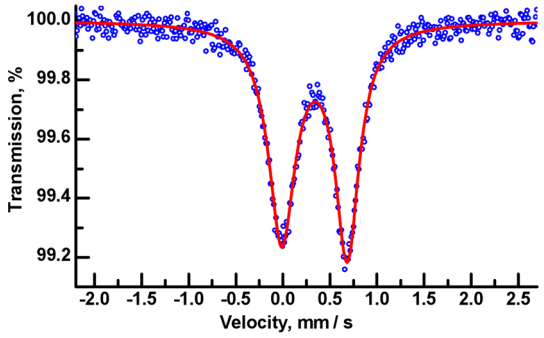

Figure 9. Mössbauer spectrum collected at room temperature. Circles are the experimental data, the solid line is calculated.

High Frequency Electron Paramagnetic Resonance (HF-EPR) Spectroscopy. In the HF-EPR spectra the signals originating from a quintet spin state (S = 2) were easily identified (Figure 10). The spectra were interpreted using the spin Hamiltonian

dx.doi.org/10.1021/ic301460q | Inorg. Chem. 2012, 51, 9110−9122

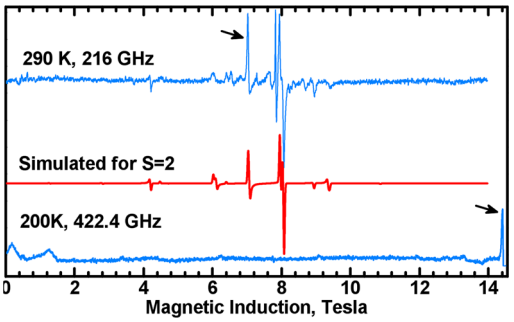

Figure 10. HF-EPR spectra of **1**. Top: experimental spectrum at 290 K, taken with 216.0 GHz. Center: Simulation assuming $S = 2$ with $g_x = 2.015$, $g_y = 2.011$, $g_z = 2.012$, $D = 1.029$ cm^{-1}, $E = 0.008$ cm^{-1}, $B_4^0 = -0.0014$ cm^{-1}, $B_4^4 = -0.0002$ cm^{-1}. Bottom: Resonances attributed to the triplet spectrum ($S = 1$) appear at very low magnetic fields at microwave frequencies 406–435 GHz and are better observed at moderately lowered temperature. The estimated D parameter in the triplet state is 13.9 cm^{-1}. The arrows indicate a characteristic line in the $S = 2$ spectrum shifting with the microwave frequency.

$$\hat{H}_S = \mu_B B\cdot g\cdot \hat{S} + D\{\hat{S}_z^2 - S(S+1)/3\} + E(\hat{S}_x^2 - \hat{S}_y^2) + B_4^0 O_4^0 + B_4^4 O_4^4$$

in which the zero-field splitting parameters are different in each coupled-spin state S. The following parameters were found from the simulation procedures: $g_x = 2.015$, $g_y = 2.011$, $g_z = 2.012$, $D = 1.029$ cm^{-1}, $E = 0.008$ cm^{-1}, $B_4^0 = -0.0014$ cm^{-1}, $B_4^4 = -0.0002$ cm^{-1}. The zero-field splitting parameters for $S = 2$ are considerably larger in this complex than in other binuclear iron(III) complexes.[13] The triplet state was difficult to detect. At very high microwave frequencies, 406 to 435 GHz, a resonance was seen at very low magnetic fields (Figure 10, bottom). That resonance first moved toward lower magnetic field when the frequency was increased from 406 GHz (lower limit in the 400 GHz range of our system), appeared to cross the zero magnetic field around 416 GHz, and then moved toward higher magnetic field. This behavior allowed to assign this resonance to the triplet state and to estimate the triplet state D value to be about 13.9 cm^{-1}, also much larger than in other iron(III) dimers.[13e–g]

The zero-field splitting parameters observed in various spin states contain contribution due to the anisotropic interactions between the two ions as well as a contribution related to the zero-field splitting on separate high-spin Fe(III) ions. They can be expressed as

$$D_S = \alpha_S D_e + \beta_S D_c, \qquad E_S = \alpha_S E_e + \beta_S E_c$$

where the index S designates a coupled-spin state (1, 2,...), D_e and E_e are the interaction parameters, while D_c, E_c refer to the zero-field splitting of the $S = 5/2$ state of each of the two iron ions. For a system of two $S = 5/2$ ions, $\alpha_1 = 3.7$, $\beta_1 = -6.4$, $_2 = 41/42$, $\beta_2 = -20/21$ and D_c, D_e can be evaluated.[13,14] The EPR data were not sufficient to determine the signs of D in the triplet and quintet states, and two possibilities have to be considered. Assuming that D in the triplet and quintet states have the same sign, one obtains $|D_c| = 3.6$ cm^{-1} and $|D_e| = 2.4$ cm^{-1}. If the signs are different then $|D_c| = 6.4$ cm^{-1} and $|D_e| = 7.3$ cm^{-1}. D_e includes contributions from both the magnetic dipole–dipole interactions and the anisotropic exchange interactions. The dipolar part is $D_e^{\text{dipolar}} = -3g_z^2\mu_B^2/R^3$, where R is the inter-ion distance, $R = 3.1567$ Å, resulting in -0.11 cm^{-1}. D_e^{dipolar} is apparently much too small to explain the magnitude of D_e and the anisotropic exchange interactions must contribute to the zero-field splitting.

ESI Mass Spectrometry. Electrospray ionization mass spectroscopy (ESI-MS) was used as a convenient solution-based technique to examine the behavior of **1** in solution with the aim of screening possible transformation processes and detecting any novel species formed. The investigation of diluted (ca. 1×10^{-5} M) solutions of **1** in acetonitrile shows only one major product of decomposition: $[Co(HSae)_2]^+$ at 387.0 m/z. The negative mode spectra revealed a number of peaks of very low intensity, whose compositions were not identified. The particle $[Co(HSae)_2]^+$ is expected if one considers the proposed formation scheme of **1** (Figure 6), the other proposed intermediates either form uncharged species, or decompose in solution. However, careful examination of the spectra allowed to find a peak at 825.7 m/z (ca. 4% of peak intensity) that could be attributable to a trinuclear particle $[Co_2Fe(Sae)_4]^+$, which represents one-half of the dimeric hexanuclear structure of **1**, while the molecular peak of **1** was not detected in any spectrum.

The peak intensities ratio $[Co(HSae)_2]^+$: $[Co_2Fe(Sae)_4]^+$ was found to be dependent on the overall concentration of **1** in solution (Supporting Information, Figures S5–S7). With increasing concentration of **1**, the intensity of $[Co_2Fe(Sae)_4]^+$ increases, reaching about 35% of the $[Co(HSae)_2]^+$ peak intensity for $[\mathbf{1}] = 3 \times 10^{-5}$ M. This spectrum showed a number of other peaks of lower intensity, whose compositions were not identified, although the isotopic distribution suggested their polynuclear nature. Since the solubility of pure **1** in acetonitrile is limited to about 3×10^{-5} M, the further ESI-MS tests were performed by using an acid promoter with the final concentration of 0.04 M or lower. These conditions are related to those employed in the catalytic experiments (see below). With the acid, only two major peaks at 387.0 and 825.7 m/z were detected, while all the others seem to be suppressed. The solution with $[\mathbf{1}] = 2 \times 10^{-5}$ M shows about 5% of $[Co_2Fe(Sae)_4]^+$ (compared to $[Co(HSae)_2]^+$, 100% peak in all spectra). The increase of the concentration of **1** to 5×10^{-5} M and 1×10^{-4} M leads to 14 and 23% of $[Co_2Fe(Sae)_4]^+$ peaks intensities, respectively.

Catalytic Oxidation of Alkanes. We investigated the catalytic potential of compound **1** for the oxidation of various alkanes by aqueous hydrogen peroxide under mild conditions. The reaction occurs in acetonitrile solution, and nitric acid in low concentration is a necessary component of the reaction mixture. Sulfuric acid has a weaker accelerating effect, whereas oxalic, hydrochloric, and trifluoroacetic acids are absolutely inactive. No alkane oxidation products (or only traces) were obtained in the absence of any component of the catalytic system: catalyst, nitric acid, or hydrogen peroxide (Scheme 1; n = 1, 3). The reaction gives alkyl hydroperoxides which are gradually transformed into the corresponding ketones (aldehydes) and alcohols (the oxidation of cyclic alkanes is presented in Scheme 1). To estimate the concentrations of the

Scheme 1

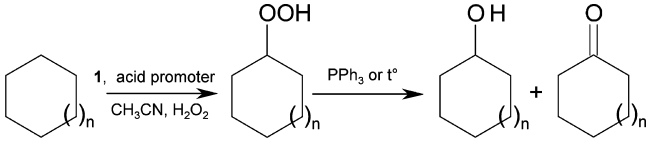

dx.doi.org/10.1021/ic301460q | Inorg. Chem. 2012, 51, 9110–9122

three products we measured the concentrations of the ketone and alcohol twice, before and after the addition of PPh_3 in accord with the method developed earlier by some of us.[15]

An example of kinetic curves in the oxidation of cyclooctane is shown in Figure 11. After 6 h the yield of oxygenates attained

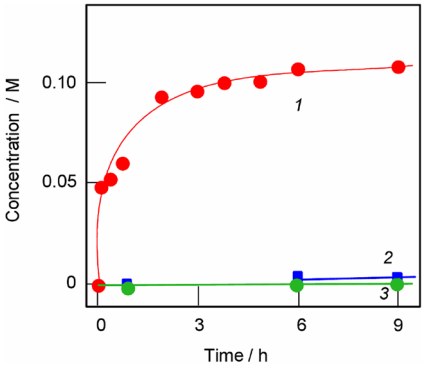

Figure 11. Accumulation of oxygenates (cyclooctyl hydroperoxide, curve *1*; cyclooctanone, curve *2*; cyclooctanol, curve *3*) with time in cyclooctane (0.25 M) oxidation with H_2O_2 (1.0 M, 50% aqueous) catalyzed by complex **1** (5×10^{-5} M) in the presence of HNO_3 (0.04 M, 65% aqueous) in acetonitrile (total volume of the reaction solution was 5 mL), 50 °C.

46% based on cyclooctane and turnover number (TON, turnover number, moles of products per mol of catalyst precursor) was 2.28×10^3. The dependence of the product yield after 5 h in the cyclohexane oxidation on catalyst concentration is depicted in Figure 12. The curve exhibits a

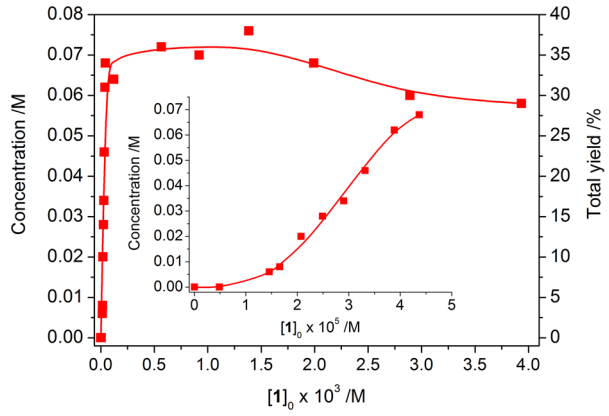

Figure 12. Effect of the catalyst concentration on the total yields of cyclohexanol and cyclohexanone (determined by GC after reduction with PPh_3) in the oxidation of cyclohexane with H_2O_2 (1.0 M, 30% aqueous) catalyzed by complex **1** in the presence of HNO_3 (0.04 M, 65% aqueous) in acetonitrile (total volume of the reaction solution was 5 mL), room temperature, 5 h reaction time. The inset shows the $[\mathbf{1}]_0 = (0-5) \times 10^{-5}$ M region in detail.

steep ascent in the low concentration region (1×10^{-5} M < $[\mathbf{1}]_0$ < 5×10^{-5} M), then reaching a plateau with a slight decrease at the concentrations of **1** higher than 2×10^{-3} M (because of the overoxidation). The highest total yield of 38% was achieved for catalyst concentration of 1.4×10^{-4} M and H_2O_2/catalyst ratio of 36: 1 (Table 1,Entry 1). The highest overall TON of 1.6×10^3 (Figure 13) was obtained for $[\mathbf{1}]_0 = 3.9 \times 10^{-5}$ M, with the overall yield of 31% (Table 1, Entry 2).

An increase of cyclohexane concentration results in the increase of the overall TON with a nearly linear dependence (Figure 14) at the initial stage. The saturation of the reaction mixture by cyclohexane ($[CyH]_0$ = 0.6 M) gives the highest overall TON of 3.57×10^3 (Table 1, Entry 6), but a further rise of the substrate amount leads to a rapid yield decrease (16% for [CyH] ≈ 0.8 M; Table 1, Entry 7). The usage of 50% H_2O_2 instead of 30% (the final concentration of H_2O_2 was 1.75 M instead of 1 M, respectively) had no influence on the above dependence.

It should be emphasized that yields up to 40% in the oxidations of very inert alkanes can be considered as very high.[5,6,15,16] The TONs of about 1600−3600 obtained in the case of catalysis by **1** are much greater than the typical values of 20−200. Moreover, the combination of such a high yield (up to 40%) and TON is rare and indicates an exceptional activity of the catalytic system based on complex **1**. Usually high TON values, up to 1500, correspond to a yield lower than 5% based on substrate.[16c]

Data on the oxidation of the linear alkanes *n*-heptane and *n*-octane, and the branched cycloalkane methylcyclohexane are summarized in Supporting Information, Tables S4, S5, and S6 (see also Supporting Information, Figure S8). Regio-[C(1):C(2):C(3):C(4)] and bond [1°: 2°: 3°] selectivity parameters given in Supporting Information, Tables S4 and S5 (see refs 17−19) are low which allows us to assume that the oxidizing species in these reactions is the hydroxyl radical. Supporting Information, Table S6 (entries 2−7) includes, for comparison, selectivity parameters for some other systems based on H_2O_2. All these systems are known to oxidize alkanes with the participation of hydroxyl radicals.

The kinetic data of the cyclohexane oxidation presented in Figure 15 are also in agreement with the assumption of the participation of hydroxyl radicals in the alkane oxygenation.

The mode of dependence of the initial cyclohexane (CyH) oxidation rate W_0 on the initial cyclohexane concentration (W_0 is approaching to a plateau at high concentrations of cyclohexane, see Figure 15A) can be explained by the competitive interaction of hydroxyl radicals both with cyclohexane and acetonitrile.[18] The following kinetic scheme describes the dependence of W_0 on $[\text{cyclohexane}]_0$:

$$H_2O_2 + \mathbf{1} \rightarrow HO\bullet \qquad (\text{rate } W_i) \tag{1}$$

$$HO\bullet + CyH \rightarrow Cy\bullet \rightarrow \rightarrow CyOOH \qquad (\text{constant } k_2) \tag{2}$$

$$HO\bullet + MeCN \rightarrow \rightarrow \text{products} \qquad (\text{constant } k_3) \tag{3}$$

where the initiation stage (1) corresponds to the catalytic generation of hydroxyl radicals with rate W_i, the stages (2) correspond to the sequence of transformations of CyH into CyOOH (with kinetically rate-limiting interaction between HO• and CyH), and the stage (3) is the reaction of HO• with acetonitrile.

The analysis of this kinetic scheme in the quasi-stationary approximation relative concentration of hydroxyl radicals leads to the following equation:

$$-\frac{d[CyH]}{dt} = \frac{d[CyOOH]}{dt} = \frac{W_i}{1 + \frac{k_3[MeCN]}{k_2[CyH]}} \tag{4}$$

dx.doi.org/10.1021/ic301460q | Inorg. Chem. 2012, 51, 9110−9122

Table 1. Oxidation of Cyclohexane with Hydrogen Peroxide to the Corresponding Cyclic Alcohols and Ketones Catalyzed by Complex 1.[a]

				yields[b] of products obtained from CyH, %			
entry	[CyH], M	$n(H_2O_2)/n(CyH)$	[1] × 10^5, M	ketone	alcohol	total	TON[c]
1	0.2	5.0	14	6	32	38	543
2[d]	0.2	5.0	14	20	11	31	443
3	0.2	5.0	3.9	2	29	31	1.60 × 10^3
4[d]	0.2	5.0	3.9	20	7	26	1.34 × 10^3
5	0.6	1.67	4.4	3	23	26	3.57 × 10^3
6[d]	0.6	1.67	4.4	15	9	23	3.20 × 10^3
7	0.8[e]	1.25	4.4	1	15	16	2.83 × 10^3
8[f]	0.37	2.7	11	3	18	21	722

[a]Selected data; reaction conditions (unless stated otherwise): catalyst precursor, H_2O_2 (1.0 M, 30% aqueous), CyH (0.2 M), HNO_3 (0.04 M, 65% aqueous), acetonitrile (total volume of the reaction solution was 5 mL), 5 h reaction time, ambient temperature (ca. 20 °C). [b]Moles of product/100 mols of cyclohexane, measured upon reduction of the reaction mixture by PPh_3 (ROOH is transformed to the alcohol ROH). [c]Overall TON values (mols of products per mol of catalyst). [d]Yields measured prior to addition of PPh_3 (for comparative purposes). [e]Total amount of cyclohexane in the catalytic system (the real concentration is limited by solubility to ca. 0.6 M). [f]Accumulation within 15 min under the following conditions: catalyst precursor, H_2O_2 (1.0 M, 50% aqueous), CyH (0.37 M), HNO_3 (0.04 M, 65% aqueous), acetonitrile (total volume of the reaction solution was 5 mL), 50 °C.

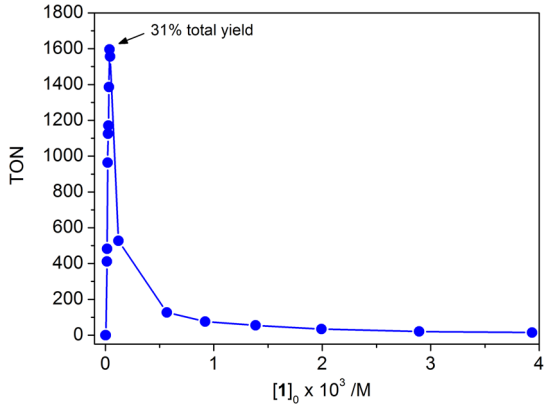

Figure 13. Effect of the catalyst concentration on the overall TON (turnover number; mols of products/mol of catalyst). The conditions are the same as described for Figure 12.

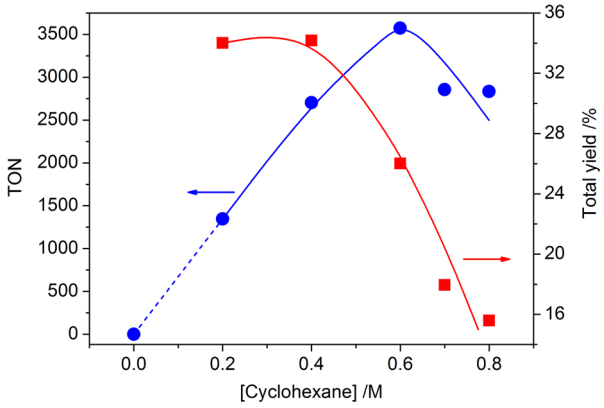

Figure 14. Effect of the cyclohexane (CyH) concentration on the total yields of cyclohexanol and cyclohexanone (red) and total TONs (blue) in the oxidation of cyclohexane with H_2O_2 (1.0 M, 30% aqueous) catalyzed by complex **1** (4.4 × 10^{-5} M) in the presence of HNO_3 (0.04 M, 65% aqueous) in acetonitrile at room temperature, 5 h reaction time. Total initial volume of the reaction solution was 5 mL, taking into account the limited solubility of cyclohexane in acetonitrile. For the tests with $[CyH]_0$ > 0.4 M a complete dissolution of cyclohexane was observed in about 30 min.

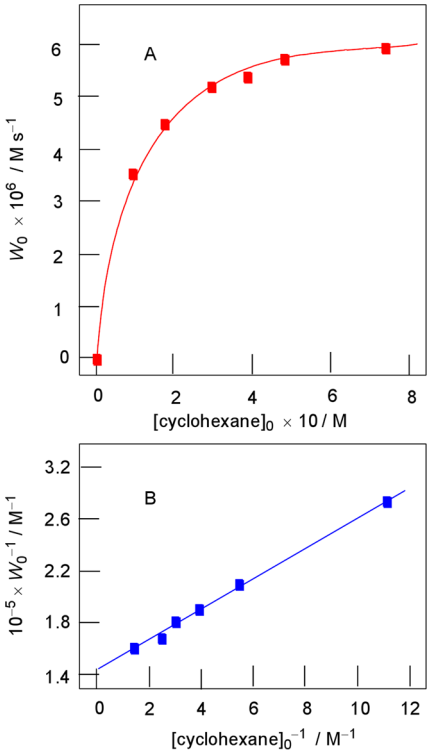

Figure 15. Oxidation of cyclohexane with hydrogen peroxide (1.0 M, 50% aqueous) catalyzed by compound **1** (3.2 × 10^{-5} M) in the presence of HNO_3 (0.04 M, 65% aqueous) in MeCN at 50 °C. Graph A: dependence of the initial rate of oxygenate formation W_0 on initial concentration of cyclohexane. Graph B: anamorphosis of curve shown in Graph A in coordinates $[cyclohexane]_0^{-1} - W_0^{-1}$. Concentrations of oxygenates (sum of cyclohexanol and cyclohexanone) were measured after reduction with PPh_3.

In accordance with eq 4 for the initial fragments of the kinetic curves, the term

$$\frac{1}{\frac{d[CyOOH]}{dt}}$$

should be a linear function of $1/[CyH]_0$. The experimental data are in agreement with this dependence which is shown in

dx.doi.org/10.1021/ic301460q | Inorg. Chem. 2012, 51, 9110−9122

Figure 15B. This dependence allows us to determine the following ratio:

$$\frac{k_3[\mathrm{MeCN}]}{k_2} = 8 \times 10^{-2}\ \mathrm{M}$$

Assuming [MeCN] = 18 M in the reaction solution, we obtain $k_3/k_2 = 4.4 \times 10^{-3}$. Values $k_3[\mathrm{MeCN}]/k_2$ (8×10^{-2} M) and k_3/k_2 (4.4×10^{-3}) are close to the corresponding parameters obtained by some of us for oxygenation of cyclohexane in acetonitrile with H_2O_2 catalyzed by the systems Cp^*_2Os/py ($\{9\div20\} \times 10^{-2}$ M and $\{5\div11\} \times 10^{-3}$),[19a] VO_3^-/PCA (15×10^{-2} M and 8.3×10^{-3}),[19b] $Fe(ClO_4)_3$ (12×10^{-2} M and 7×10^{-3}),[18c] a binuclear iron(III) complex with 1,4,7-triazacyclononane/PCA (20×10^{-2} M and 11×10^{-3}).[18c] These parameters, measured for other systems, for example, for the photochemical oxidation of cyclohexane with H_2O_2 (23.4×10^{-2} M and 13×10^{-3})[18c] and radiation-chemical experiments (21.6×10^{-2} M and 12×10^{-3}),[18c] are comparable with those obtained in the oxidation catalyzed by **1**. For all these reactions the hydroxyl radical is known to be the oxidant.

In the cyclohexane oxidation, the dependence of the initial reaction rate (W_0 = d[CyOOH]/dt) on concentration of **1** introduced into the reaction solution (Figure 16A) testifies that the reaction order is higher than first order relative to **1**. The ESI-MS tests (see above) showed two major particles, $[Co(HSae)_2]^+$ and $[Co_2Fe(Sae)_4]^+$, formed in the solutions of **1**, and the ratio of their concentrations depend on the overall concentration of **1** (the higher [**1**], the higher $[Co_2Fe]$). Considering these results, the assumption was made that the trinuclear Co_2Fe particle is responsible for the intensive growth of the initial reaction rate starting from the [**1**] ~ 3×10^{-5} M (Figure 16). Let us consider that monomeric (**M**) cobalt (**Co**) and trimeric (**T**, of Co_2Fe type) species are formed from the initial hexameric molecules **1** (while the whole molecule of **1** has not been detected in the solution). In accordance with this observation we can write the following material balance equation:

$$6 \times [\mathbf{1}]_0 = [\mathbf{Co}] + [\mathbf{Fe}] + 3 \times [\mathbf{T}] \qquad (5)$$

Here $[\mathbf{1}]_0$ is the concentration of starting hexameric complex **1**, $6 \times [\mathbf{1}]_0$ corresponds to the maximum concentration of the monomeric species with the cobalt and iron ions generated from **1**, [Co] and [Fe] is equal to the real concentrations of the monomeric species with the cobalt and iron ions in the solution, and $3 \times [\mathbf{T}]$ is equal to the concentration of monomeric species formed when the trimeric complex **T** completely dissociates.

It is clear that the concentration of Co ions in the solution is two times higher than the concentration of ions Fe, that is [**Co**]/[**Fe**] = 2. A portion of ions is present in the form of the monomers **Co** and **Fe**, and another portion exists as the trimers **T**. Let us introduce the effective equilibrium constant K for the equilibrium in the formation of trimers from monomers:

$$2\mathbf{Co} + \mathrm{Fe} \rightleftarrows \mathbf{T} \qquad (K = [\mathbf{T}]/[\mathbf{Co}]^2[\mathbf{Fe}]) \qquad (6)$$

Denoting [**Fe**] as [**M**] and taking into account that [**Co**]/[**Fe**] = 2 we can rewrite eq 6 in the form:

$$K = [\mathbf{T}]/4[\mathbf{M}]^2 \qquad (6a)$$

The data presented in Figure 16 demonstrate that the catalytic activity of the trimers is many times higher than that of the monomers. Thus, let us assume that in the whole studied interval of the hexamer concentrations the initial oxidation rate is

$$W_0 = k_{\mathrm{eff}}[\mathbf{T}] \qquad (7)$$

The effective rate constant k_{eff} is in particular a function of $[H_2O_2]$. In this case, with $[H_2O_2]$ = *const*, it follows from eqs 6a and 7 that

$$\mathbf{M} = \left(\frac{W_0}{4k_{\mathrm{eff}}K}\right)^{1/3} \qquad (8)$$

which means that

$$6 \times [\mathbf{1}]_0 = \left(\frac{W_0}{4k_{\mathrm{eff}}K}\right)^{1/3} + 3\frac{W_0}{k_{\mathrm{eff}}} \qquad (9)$$

Let us transform eq 9 into the following form:

$$\frac{[\mathbf{1}]_0}{W_0^{1/3}} = a + bW_0^{2/3} \qquad (10)$$

where

$$a = \frac{1}{2(4k_{\mathrm{eff}}K)^{1/3}} \quad \text{and} \quad b = \frac{1}{2}\frac{1}{k_{\mathrm{eff}}}$$

The linear anamorphosis of the experimental dependence (Figure 16A) calculated in accord with eq 10 is shown in Figure

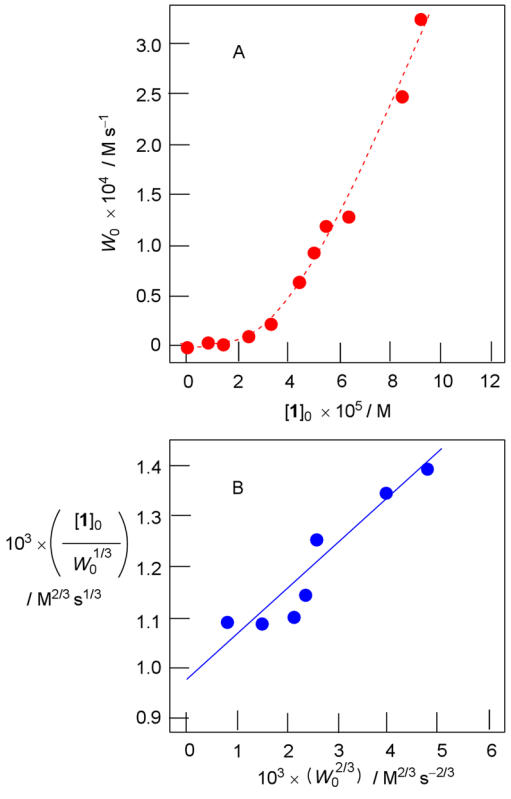

Figure 16. Oxidation of cyclohexane (0.37 M) with hydrogen peroxide (1.0 M, 50% aqueous) catalyzed by compound **1** in the presence of HNO_3 (0.04 M, 65% aqueous) in MeCN at 50 °C. Graph A: dependence of the initial rate of oxygenate formation W_0 on initial concentration of **1**. Graph B: the anamorphosis of curve shown in Graph A in coordinates $[\mathbf{1}]_0/W_0^{1/3} - W_0^{2/3}$. Concentrations of oxygenates (sum of cyclohexanol and cyclohexanone) were measured after reduction with PPh_3.

dx.doi.org/10.1021/ic301460q | *Inorg. Chem.* 2012, 51, 9110–9122

16B. It can be seen that the experimental data are in a tolerable agreement with eq 10. The data presented in Figure 16B yield parameters $a = 0.95 \times 10^{-3}$ $M^{2/3}$ $s^{1/3}$ and $b = 0.096$ s, and, consequently, under the conditions of our experiment, $k_{eff} = 1/(2b) = 5.2$ s^{-1} and $K \approx 7 \times 10^6$ M^{-3}. The simulation of the dependence of W_0 on $[\mathbf{1}]_0$ using eq 10 and parameters a and b given above produced the dashed-line curve in Figure 16A which demonstrates good agreement between calculated and experimental values W_0 at different initial concentrations of **1**.

For solutions with the initial concentration of **1** equal to 1.1×10^{-4} M the value of W_0 was found to be 3.44×10^{-4} M s^{-1}. Using the above coefficient $k_{eff} = 5.2$ s^{-1} one can find $[\mathbf{T}] = 6.6 \times 10^{-5}$ M and, furthermore, the constant $K \approx 7 \times 10^6$ M^{-3} allows us to estimate $[\mathbf{Co}] + [\mathbf{Fe}] = 4 \times 10^{-4}$ M in the solution. In all ESI-MS spectra we observe only one type of monomeric species, namely, $[Co(HSae)_2]^+$, while the monomeric iron species were not detected. Thus, the concentration of cobalt-only particles is $[\mathbf{Co}] = 2.7 \times 10^{-4}$ M. The final $[\mathbf{T}]/[\mathbf{Co}]$ ratio of 0.24 for $[\mathbf{1}] = 1.1 \times 10^{-4}$ M perfectly fits to observed peak intensities ratio in the respective mass-spectrum, where 0.23 ratio was found (Supporting Information, Figure S5). The analogous calculations for $[\mathbf{1}]_0 = 5.0 \times 10^{-5}$ and 1.2×10^{-5} M reveals 0.11 and 0.06 theoretical $[\mathbf{T}]/[\mathbf{M}]$ ratios, respectively. The mass-spectra of the solutions shows peak intensities ratios of 0.14 and 0.03, respectively, which are in good agreement with predicted ones. Finally, it is quite important to notice that successful fitting of the experimental data to the model with the $2\mathbf{Co} + \mathbf{Fe} \rightleftarrows \mathbf{T}$ equilibrium, as well as its correspondence with mass-spectral data, confirm our supposition that $[Co_2Fe(Sae)_4]^+$ is a catalytically active particle of the system based on **1**.

Further Mechanistic Discussion. At the concentration $[\mathbf{1}]_0 = 1.1 \times 10^{-4}$ M the initial reaction rate shows a very high turnover frequency (TOF) value of 1.12×10^4 h^{-1} (Table 1, Entry 8). This rate is comparable to one of the highest reported rates (2.4×10^4 h^{-1}), observed for an osmium-based catalytic system,[15d] and is much greater than those for an overwhelming majority of catalytic systems based on coordination compounds as precatalysts. It was shown above that such a high rate could be associated to the heterometallic particle $[Co_2Fe(Sae)_4]^+$ present in the concentrated solutions of **1**. To prove that this particle remains under the catalysis conditions, the respective solutions were investigated by ESI-MS. The addition of nitric acid and hydrogen peroxide (at room temperature) does not influence the spectra significantly. After one hour the peak intensity of Co_2Fe particle dropped from 23% to 14% for the room-temperature catalytic system with $[\mathbf{1}] = 1.1 \times 10^{-4}$ M, while the initial solution of **1** does not show significant changes with time. This stability is also supported by the fact that the catalytic activity of already prepared solutions of **1** keeps the same for a long time (more than six months).

The accumulations of products at 50 °C in the catalytic tests with $[\mathbf{1}]$ equal to 1.1×10^{-4} and 9.6×10^{-5} M (highest investigated concentrations) are shown at Figure 17. As can be seen, the reaction rate rapidly decreases with time. The quasi-linear regions of both dependencies are negligible, forcing the use of exponential fitting to evaluate the correct initial reaction rate W_0. The decrease of $[\mathbf{1}]$ leads to the increase of the initial quasi-linear region, which become evaluable for $[\mathbf{1}] < 4 \times 10^{-5}$ M, finally reaching about 1 h period for the lowest investigated concentrations.

The observed reaction rate decay could not be explained only by decrease of substrate or H_2O_2 amounts in the catalytic system, since it accumulates no more than 20% of total yield before reaching plateau (ca. 10 min; Figure 17). Hence, it is assumed that the catalyst undergoes degradation upon attack by hydroxyl radicals generated at a very high rate. Really, the catalyst contains a Schiff base ligand with numerous C–H bonds and N-atoms that can be oxidized with the subsequent change of ligand's structure and function. Also, the observation of the color of solution, changing from light-brown to colorless during the reaction, suggested the decomposition of the Schiff base group. The ESI-MS spectra of these colorless solutions showed the absence of both $[Co(HSae)_2]^+$ and $[Co_2Fe(Sae)_4]^+$ particles and, moreover, revealed no dominant peaks in the 100–2000 m/z region.

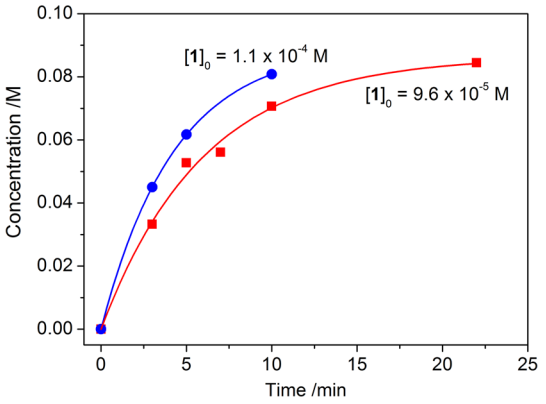

Figure 17. Accumulation of oxygenates (sum of cyclohexanol and cyclohexanone) with time in cyclohexane (0.37 M) oxidation with hydrogen peroxide (1.0 M, 50% aqueous) catalyzed by compound **1** in the presence of HNO_3 (0.04 M, 65% aqueous) in MeCN at 50 °C. Concentrations of the products were measured after reduction with PPh_3.

The UV/vis spectrum of **1** exhibits a smooth absorbance at the visible region with one notable maximum at 388 nm, $\varepsilon_{388} = 17713$ M^{-1} cm^{-1} (Figure 18). In the UV region two clear peaks, at 210 and 253 nm, are observed. The spectral pattern of **1** remains unchanged in $[\mathbf{1}] = 5.4 \times 10^{-6}$–$3.0 \times 10^{-5}$ M concentrations range (Supporting Information, Figure S9). A

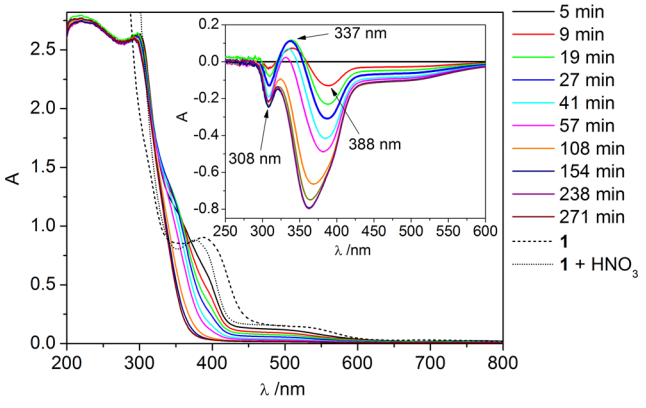

Figure 18. UV/vis spectra of acetonitrile solution of **1** (5×10^{-5} M), dashed line (---); acetonitrile solution of **1** (5×10^{-5} M) with HNO_3 (0.04 M, 65% aqueous), dotted line (···); solid lines illustrate the spectra of catalytic solutions in cyclooctane (0.25 M) oxidation with H_2O_2 (1.0 M, 50% aqueous) catalyzed by complex **1** (5×10^{-5} M) in the presence of HNO_3 (0.04 M, 65% aqueous) in acetonitrile (total volume of the reaction solution was 5 mL), 50 °C. The inset shows the difference spectra taking 5 min spectrum as the basic one.

dx.doi.org/10.1021/ic301460q | Inorg. Chem. 2012, 51, 9110–9122

further increase of concentration is limited by solubility of **1** in acetonitrile and can be enhanced only with the usage of small amounts of acid promoter (ca. 4×10^{-3} M of HNO_3 was used for spectral investigations). However, the acid causes minor spectral changes (Figure 18), such as a blue shift of the 388 nm peak to 377 nm with a slightly lower molar extinction coefficient. The UV region for concentrations of **1** higher than 3.0×10^{-5} M can not be evaluated because of very strong absorption. To clarify the color changes of the catalytic systems (from light-brown to colorless), the UV/vis spectra of the cyclooctane catalytic system, under conditions similar to those described above (Figure 14), were monitored (catalyst concentration was $[\mathbf{1}] = 5.1 \times 10^{-5}$ M, all other parameters remained the same). The dependence of the spectral pattern on the time, as well as the respective UV/vis spectra of pure **1** and **1** + HNO_3 in acetonitrile, are depicted at Figure 18. As can be seen, the main changes occur in the 250−600 nm region (Figure 18, inset). The intensity of the 388 nm peak, typical for **1**, continuously decays with the time, thus confirming the decomposition of the compound **1** under the present catalytic conditions. In 4.5 h time the spectrum reaches a plateau that corresponds to the colorless, catalytically inactive solution. The ESI-MS spectra of the 50 °C catalytic test with various concentrations of **1** revealed no considerable peaks in the 100−2000 m/z region after the solution became colorless, pointing to a complete decomposition of all coordination species under elevated temperatures.

Surprisingly, the absorbance at 337 nm was found to be in nonlinear dependence on the reaction time (Figures 18, 19). In

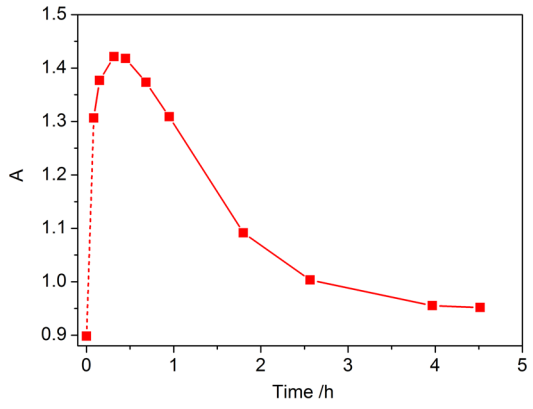

Figure 19. Variation of absorbance (A) at 337 nm with the time for a catalytic solution of **1** (the conditions are the same as described for Figure 18). The first point belongs to a pure solution of **1** (5×10^{-5} M) in acetonitrile.

the period from 5 to 20 min from the beginning the peak reaches a maximum intensity, being stable for about 10 min, and then quickly falls to the background absorption level (Figure 19). Moreover, one could notice some conformity between the intensity of the 337 nm peak and the reaction rate: the period showing the highest reaction rate (ca. until 30 min) corresponds to the highest intensity of this peak, while the further rate decay is in agreement with the respective decay of the 337 nm peak intensity. Although the initial reaction rate was always observed to be the highest one for all the reaction conditions (this contrasts with the increase of the 337 nm peak in the 0−20 min range), one can suppose that this absorption corresponds to an intermediate compound, a component of the reaction solution. Unfortunately, it is not possible to assign this peak to some definite compound because of the great complexity of the catalytic system—the absorbance at about 330 nm could be due to organic species or charge transfer in cobalt or iron coordination compounds, including peroxo- and hydroxyperoxo species of these metals.[20]

Although the hydroxyl radicals were proved to be the main attacking particles in the present catalytic systems, the question about the catalytic mechanism in general remains open. In spite of the fact that the catalytic reactions of transition metal compounds with hydrogen peroxide have been investigated for more than a century, the great complexity of these Fenton-like processes[21] still does not allow reliable predictability of such reactions. In the classical Fenton reagent, the first stage is the decomposition of hydrogen peroxide to hydroxyl radical and hydroxyl anion:[21d]

$$Fe^{2+} + HOOH \rightarrow Fe^{3+} + HO\cdot + OH^-$$

The hydroxyl radical interacts further with the C−H bond to form the respective alkyl radical:

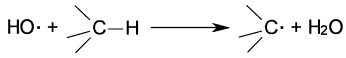

The first stage has a high activation barrier illustrated by the rate constant of only 76 M^{-1} s^{-1}, while, for example, cyclohexanone reacts with the hydroxyl radical with the much higher rate of 6×10^9 M^{-1} s^{-1}.[21d] Thus, a huge number of the catalytic systems, including that based on **1**, differ only by efficiency of the initiation reaction of the coordination compound with HOOH or *t*-Bu-OOH.

In the present case, the combination of high yield and TON for cyclohexane (26% and 3.57×10^3, respectively, for Table 1, Entry 5), as well as the high TOF of 1.12×10^4 h^{-1} (Table 1, Entry 8), was associated to the trimetallic particle $[Co_2Fe(Sae)_4]^+$ which, probably, is the highly efficient initiator of the HO• generation. It was shown earlier[15,18c,22] that the presence of polydentate ligands has a prominent influence on the catalytic activity of iron ions under conditions close to that for **1**, enhancing the reaction rate up to 10^3 times.[15,18c,22] The $Co(Sae)_2$ blocks also could be viewed as a bidentate ligand, participating in square-pyramidal coordination environment around iron atom in **1**, as evidenced by single crystal X-ray analysis (Figure 1). However, according to ESI-MS data the axial oxygen atom decoordinates in solution, and it is most probable that in the $[Co_2Fe(Sae)_4]^+$ particle the $Co(Sae)_2$ blocks form a tetracoordinated environment. The geometry of such environment could range from nearly square planar (square pyramid without axial bonding) to tetrahedral. The coordination of the third $Co(Sae)_2$ block is less probable because of the steric hindrance of the bulky Sae ligands; also this contrasts to ESI-MS data. Such a coordination environment is unsaturated and in this way the iron center could actively participate in catalytic processes. Since the activation of hydrogen peroxide by a metal ion is the limiting stage, one could propose a few possibilities that make the $[Co_2Fe(Sae)_4]^+$ particle especially active in this reaction. First, a stable, unsaturated coordination geometry could stipulate specific coordination of hydrogen peroxide to the iron metal center. This may include additional hydrogen bonding of HOOH with the deprotonated hydroxyl groups of the aminoalcohol ligand, located in close proximity. Furthermore, these ligands could serve as a proton-transfer device, forcing the abstraction of the proton from the hydrogen peroxide, as was observed previously for some N-donor ligands.[22] One can notice that the nitrate

dx.doi.org/10.1021/ic301460q | *Inorg. Chem.* 2012, 51, 9110−9122

Table 2. Selectivity Parameters in Oxidations of Alkanes with *m*-CPBA Catalyzed by Complex 1[a]

		C(1):C(2):C(3):C(4)	1°:2°:3°	*trans*/*cis*	
entry	$[HNO_3]$, M	*n*-heptane	MCH	*cis*-1,2-DMCH	*trans*-1,2-DMCH
1	0	1:88:61:105	1:180:860	0.7	1.0
2	0.02	1:190:230:220	1:130:2130	0.06	8.5

[a]Conditions: $[\mathbf{1}]_0 = 5 \times 10^{-5}$ M, solvent MeCN, 23 °C, 22 h. Selectivity parameters were determined on the basis of concentrations of alcohol and ketone isomers after reduction with PPh_3.

anion could also play a special role, since the catalytic system based on **1** possesses weak or no activity in the absence of nitric acid. Although the above scheme considers the cobalt $Co(Sae)_2$ block only as a bulky ligand, one can suppose at least few possibilities of Co^{III} ions to participate in the oxidation reaction mechanism. This may include Ox-Red reactions between cobalt and iron ions (when one of the ions is in the reduced state) or interaction of cobalt and peroxo-species by decoordinating one of the bridging μ-O atoms from the deprotonated amino-alcohol.

We have also found that cyclohexane (0.25 M) in the presence of complex **1** (5×10^{-5} M) and HNO_3 (0.02 M) in acetonitrile solution (total volume 5 mL) can be oxidized by *m*-chloroperoxybenzoic acid (*m*-CPBA, 45 mg) to afford (after reduction with PPh_3) cyclohexanone (0.01 M) and cyclohexanol (0.009 M). The reaction in the absence of nitric acid was much less efficient and gave cyclohexanone (0.003 M) and cyclohexanol (0.002 M) (Table 2, Entry 1). The selectivity parameters for the oxidations by these systems of normal and branched alkanes are summarized in Table 2. The oxidation of isomeric 1,2-DMCH (DMCH = dimethylcyclohexane) exhibited a very remarkable peculiarity: the reaction is highly stereoselective, but only in the presence of nitric acid. The selectivity parameters dramatically differ from those obtained for the reactions with H_2O_2 (compare with the data of Supporting Information, Table S6) which indicates that in the case of *m*-CPBA the reaction proceeds without the participation of free radicals. As in the oxidation with H_2O_2 nitrate anions are required for the creation of efficient catalytically active species. The oxidation of benzene with H_2O_2 catalyzed by **1** in the presence of HNO_3 at 50 °C (2 h) was not efficient, and phenol was formed with TON of only 27.

CONCLUSIONS

We have shown that application of the "Direct Synthesis" method together with the use of a polydentate Schiff base ligand, such as salicylidene-2-ethanolamine, represents an excellent strategy for the synthesis of polynuclear heterometallic complexes of uncommon structure. As evidenced by the searches in the CSD, the coordination core of **1** is an extremely rare example of the $M_6(\mu\text{-X})_9$ MST, where two trinuclear $M_3(\mu\text{-X})_4$ species are linked by single $M(\mu\text{-X})M$ bonding into the hexanuclear assembly.

To understand why such an unusual structure is formed, we explored possible reaction pathways and proposed a speculative mechanism for the synthesis of **1** in solution. Unfortunately, nowadays such synthetic systems usually are not subject of investigation, and even tentative discussions of how the polynuclear species are formed from multicomponent systems are quite rare.[2c] In the present case we introduced a respective scheme and, moreover, two particles present from this scheme were observed in ESI-MS spectra of the solutions of **1**.

The magnetic properties of **1** revealed an antiferromagnetic coupling between Fe(III)−Fe(III) centers. The HF-EPR spectra showed uncommon parameters for an iron dimer. These investigation methods, together with the Mössbauer spectroscopy and charge balance calculations, unambiguously define the metal oxidation states in **1** as Co(III) and Fe(III).

The catalytic data revealed an exciting activity of **1** in the mild oxidation of alkanes by hydrogen peroxide. Complex **1** is, probably, the most active coordination compound among those with N,O-donor ligands, as evidenced by achieved combinations of the overall yield(%)/TON of $31/1.60 \times 10^3$ and $26/3.57 \times 10^3$ (for oxidation of cyclohexane), whereas related catalytic systems typically could show, as most, either a high yield or a high TON. The advantages of the catalyst **1** also lie in the great TOF values, with the highest observed value of 1.12×10^4 h^{-1} (3.1 s^{-1}). We tried to understand the nature of active attacking species and found that hydroxyl radicals react with alkanes to form the respective alkyl radicals. Thus, the catalytic system belongs to the class of Fenton-like systems where the reaction of a coordination compound (solvated metal ion in the simplest case) with oxidizer (peroxide) is the initial, principal stage. By employing ESI-MS techniques together with kinetic experimental data we were able to assume that the $[Co_2Fe(Sae)_4]^+$ particles, present in concentrated solutions of **1**, are the catalytically active species, responsible for the quite fast generation of hydroxyl radicals in the catalytic system.

The proposed catalytic system provides a rare example of application of a heterometallic coordination compound in homogeneous catalysis and, to the best of our knowledge, is the first case when the catalytic activity is directly associated to a heterometallic species. Although the detailed mechanism of the present system has yet to be established, we suppose that the high activity of the $[Co_2Fe(Sae)_4]^+$ particle could be due to the specific coordination environment of a tetracoordinated iron center, as well as to other effects such as hydrogen-bonded assistance and Co−Fe Ox-Red interactions. We expect that the results obtained within the present research would improve the understanding of oxidation processes and inspire further development of highly efficient catalysts for mild hydrocarbon functionalization.

EXPERIMENTAL SECTION

All chemicals were of reagent grade and used as received. All experiments were carried out in air. Elemental analyses for CHNS were performed by the Microanalytical Service of the Instituto Superior Técnico, and the elemental analyses for metals were performed by atomic absorption spectroscopy by the Department of Chemistry, Taras Shevchenko National University of Kyiv. Infrared spectra (4000−400 cm^{-1}) were recorded on a BX-FT IR "Perkin Elmer" instrument in KBr pellets. UV−vis spectra were recorded using Perkin-Elmer Lambda 35 spectrometer in a 200−800 nm spectral range with 2 nm spectral resolution. Pure acetonitrile was measured as background sample. ESI-MS(+) spectra were run on a 500-MS LC Ion Trap instrument (Varian Inc., Alto Palo, CA, U.S.A.) equipped with an electrospray (ESI) ion source, using 10^{-3}−10^{-5} M solutions of **1** in methanol, acetonitrile, or DMF. A Perkin-Elmer STA-6000 model thermogravimetric analyzer was used for determination of the thermal

dx.doi.org/10.1021/ic301460q | Inorg. Chem. 2012, 51, 9110−9122

stability of complex **1**. Samples weighing 5−30 mg were heated under a dinitrogen flow of 30 mL min^{-1} from 30 to 1000 °C at a heating rate of 10 °C min^{-1}.

Synthesis of $[Co_4Fe_2OSae_8]\cdot 4DMF\cdot H_2O$ (1). Salicylaldehyde (0.53 mL, 5 mmol), 2-aminoethanol (0.3 mL, 5 mmol), and triethylamine (0.7 mL, 5 mmol) were dissolved in DMF (25 mL), forming a yellow solution, and magnetically stirred at 50−60 °C (10 min). Then, cobalt powder (0.15 g, 2.5 mmol) and $FeCl_2\cdot 4H_2O$ (0.25 g, 1.25 mmol) were added to the hot yellow solution with subsequent stirring for 6 h, until total dissolution of cobalt was observed and a dark red solution formed. Dark red crystals suitable for X-ray analysis were isolated after 1 day. Yield: 0.53 g, 42.1% (per cobalt). Elemental analysis for $C_{84}H_{102}Co_4Fe_2N_{12}O_{22}$ (M_r = 1979.24). Calcd: C, 50.98; N, 8.49; H, 5.19; Fe, 5.64; Co, 11.91. Found: C, 50.8; N, 8.3; H, 5.2; Fe, 5.7; Co, 11.9. The compound is sparingly soluble in DMSO and DMF, insoluble in water, and it is stable in air.

X-ray Structure Determination. The diffraction images from the single crystal of **1** were collected on Bruker APEX-II CCD three-circled diffractometer equipped with graphite monochromated Mo−Kα radiation (λ = 0.71073 Å) using ω- and φ-scans technique. The set of reflection intensities was obtained by integration of image frames using SAINT.[23] The intensities were corrected for polarization and Lorentz effects as well as for absorption (semiempirical method) utilizing the SADABS program.[23] The structure was solved by direct methods and refined by full matrix least-squares on F^2 in anisotropic approximation for non-H atoms using SHELXTL.[23] All hydrogen atoms were treated geometrically depending on hybridization of the parent atom and refined using the "riding model" with $U_{iso}(H)$ = $1.5U_{iso}(C)$ for CH_3 and $U_{iso}(H)$ = $1.2U_{iso}(C)$ for other groups. At the end of the structure refining, several electron density peaks, located out of the main residue, with values from 1.81 to 1.00 e Å^{-3} remained. All attempts to resolve the disorder of the mentioned water molecules were unsuccessful. On this ground, the SQUEEZE routine from PLATON was applied to modify reflection intensities corresponding to disordered water molecules.[24]

$C_{84}H_{102}Co_4Fe_2N_{12}O_{22}$, M = 1979.24, tetragonal, $I\bar{4}$, a = b = 20.9562(16), c = 22.4758(18) Å, V = 9870.5(13) Å^3, T = 173(2) K, Z = 4, D(calc) = 1.332 Mg m^{-3}, μ = 1.013 mm^{-1}, F(000) = 4104.0, Θ = 1.37−26.40°, 15403 reflections collected, 9127 reflections unique (R_{int} = 0.0301), 7521 reflections observed [$I > 2\sigma(I)$], R = 0.0393, wR = 0.1032, GoF = 1.005, largest difference peak and hole: 0.312 /−0.286 e Å^{-3}. CCDC reference number 781917.

Magnetic Measurements. The magnetic data were taken using a SQUID magnetometer (Quantum Design MPMS-XL7) operating in the RSO mode at B = 0.1 T. Raw magnetic susceptibility has been corrected for the underlying diamagnetism using an estimate of χ_{dia}/(10^{-9} m^3 mol^{-1}) = $-5M_r$ [kg mol^{-1}]. The susceptibility data were converted to the effective magnetic moment μ_{eff}.

HF-EPR Spectroscopy. HF-EPR spectra were recorded with a home-built spectrometer at the EMR facility of NHMFL.[25] The instrument is a transmission-type device in which waves are propagated in cylindrical light-pipes. The microwaves were generated by a phase-locked oscillator (Virginia Diodes) operating at a frequency of 13 ± 1 GHz and generating its harmonics, of which the 4th, 8th, 16th, 24th, and 32nd were available. A superconducting magnet (Oxford Instruments) capable of reaching a field of 17 T was employed.

Mössbauer Spectroscopy. Mössbauer spectra were collected in constant acceleration mode using a spectrometer manufactured by SEE Co Inc., Edina, Minnesota, which was equipped with a ^{57}Co/Rh gamma source purchased from Cyclotron Instruments, Mainz, Germany. A Janis (Wilmington, Massachusetts) cryostat was employed for low-temperature measurements.

Catalytic Oxidation of Alkanes. The catalyst precursor **1** and the cocatalyst HNO_3 were used in the form of stock solutions in acetonitrile. Aliquots of these solutions were added to the reaction mixtures in the oxidations of alkanes. The oxidation reactions were typically carried out in air in thermostatted Pyrex cylindrical vessels with vigorous stirring; total volume of the reaction solution was 5 mL. (***Caution!*** *The combination of air or molecular oxygen and H_2O_2 with organic compounds at elevated temperatures may be explosive.*). The reactions were stopped by cooling, and analyzed twice, that is, before and after the addition of an excess of solid PPh_3. This method was developed and used previously by some of us[15] for the analysis of the reaction mixtures obtained from various alkane oxidations. Applying this method in the present work for the oxidation of cyclooctane and cyclohexane, we demonstrate that the reaction affords predominantly the alkyl hydroperoxide as a primary product which slowly decomposes to form cyclohexanol and cyclohexanone. In our kinetic studies for precise determination of oxygenate concentrations only data obtained after reduction of the reaction sample with PPh_3 were used. A Fisons Instruments GC 8000 gas chromatograph with a DB-WAX capillary column (J&W), Perkin-Elmer Clarus 500 gas chromatograph with a BP-20 capillary column (SGE) and Perkin-Elmer Clarus 600 gas chromatograph, equipped with Perkin-Elmer Clarus 600 C mass-spectrometer (electron impact), with a BPX5 capillary column (SGE) were used for quantitative and qualitative (MS) analyses of the reaction mixtures. The parameters of all the columns are 30 m × 0.32 mm × 25 μm; helium was used as the carrier gas; the internal standards were nitromethane for kinetic tests and cycloheptanone for the other ones.

■ ASSOCIATED CONTENT

Ⓢ Supporting Information

Details of NMR, IR, TGA, ESI-MS studies; selected bond lengths and angles for crystal structure of **1**; list of CSD refcodes for $M_aX_b-X-M_cX_d$ structures; selectivity parameters in the oxidations of alkanes; discussion of the overoxidation problem in the catalysis. This material is available free of charge via the Internet at http://pubs.acs.org.

■ AUTHOR INFORMATION

Corresponding Author

*E-mail: pombeiro@ist.utl.pt (A.J.L.P.), kokozay@univ.kiev.ua (V.N.K.).

Notes

The authors declare no competing financial interest.

■ ACKNOWLEDGMENTS

This work has been partially supported by the Foundation for Science and Technology (FCT), Portugal, its PPCDT (FEDER funded) program, and projects PTDC/QUI-QUI/102150/2008 and PEst-OE/QUI/UI0100/2011; the Russian Foundation for Basic Research (Grant 12-03-00084-a). HF-EPR and Mössbauer spectra were taken at the NHMF which is funded by the NSF through the Cooperative Agreement No. DMR-0654118, the State of Florida, and the DOE. The Mössbauer instrument was purchased using the User Collaboration Grant Program UCGP 5064 funds awarded to A.O. Slovak grant agency VEGA (projects 1/0052/11 and 1/0233/12) is acknowledged for the financial support. Thanks are also due to Dr. M. Cândida Vaz (IST) and Dr. M. Conceição Oliveira (IST) for the elemental and ESI-MS analyses, respectively.

■ ABBREVIATIONS

DMF, dimethylformamide; H_2Sae, salicylidene-2-ethanolamine; DMCH, dimethylcyclohexane; *m*-CPBA, *m*-chloroperoxybenzoic acid; TON, turnover number (mols of products/mol of catalyst); TOF, turnover frequency (mols of products/mol of catalyst per second or hour)

■ REFERENCES

(1) See, for example: (a) Barron, P. M.; Son, H.-T.; Hu, C.; Choe, W. *Cryst. Growth Des.* **2009**, *9*, 1960. (b) Halper, S. R.; Do, L.; Stork, J.

R.; Cohen, S. M. *J. Am. Chem. Soc.* **2006**, *128*, 15255. (c) Zhang, H.; Yang, J.-H.; Shpanchenko, R. V.; Abakumov, A. M.; Hadermann, J.; Clerac, C. R.; Dikarev, E. V. *Inorg. Chem.* **2009**, *48*, 8480.

(2) See, for reviews: (a) Andruh, M.; Costes, J.-P.; Diaz, C.; Gao, S. *Inorg. Chem.* **2009**, *48*, 3342. (b) Tanase, S.; Reedijk, J. *Coord. Chem. Rev.* **2006**, *250*, 2501. (c) McInnes, E. J. L.; Piligkos, S.; Timco, G. A.; Winpenny, R. E. P. *Coord. Chem. Rev.* **2005**, *249*, 2577.

(3) See, for reviews: (a) Ritleng, V.; Chetcuti, M. J. *Chem. Rev.* **2007**, *107*, 797. (b) Wheatley, N.; Kalck, P. *Chem. Rev.* **1999**, *99*, 3379. (c) Mukherjee, A.; Nembenna, S.; Sen, T. K.; Sarish, S. P.; Ghorai, P. Kr.; Ott, H.; Stalke, D.; Mandal, S. K.; Roesky, H. W. *Angew. Chem., Int. Ed.* **2011**, *50*, 3968. (d) Mandal, S. K.; Roesky, H. W. *Acc. Chem. Res.* **2010**, *43*, 248.

(4) (a) Que, L.; Tolman, W. B. *Compr. Coord. Chem. II* **2004**, *8*, 1. (b) Doukov, T. I.; Iverson, T. M.; Seravalli, J.; Ragsdale, S. W.; Drennan, C. L. *Science* **2002**, *298*, 567.

(5) (a) Nesterov, D. S.; Kokozay, V. N.; Dyakonenko, V. V.; Shishkin, S. O.; Jezierska, J.; Ozarowski, A.; Kirillov, A. M.; Kopylovich, M. N.; Pombeiro, A. J. L. *Chem. Commun.* **2006**, 4605. (b) Pombeiro, A. J. L.; Kirillov, A. M.; Kopylovich, M. N.; Kokozay, V. N.; Nesterov, D. S. Patent PT 103526, 2007.

(6) Nesterov, D. S.; Kokozay, V. N.; Jezierska, J.; Pavlyuk, O. V.; Boca, R.; Pombeiro, A. J. L. *Inorg. Chem.* **2011**, *50*, 4401.

(7) (a) Wang, W.-G.; Zhou, A.-J.; Zhang, W.-X.; Tong, M.-L.; Chen, X.-M.; Nakano, M.; Beedle, C. C.; Hendrickson, D. N. *J. Am. Chem. Soc.* **2007**, *129*, 1014. (b) Semenaka, V. V.; Nesterova, O. V.; Kokozay, V. N.; Zybatyuk, R. I.; Shishkin, O. V.; Boca, R.; Shevchenko, D. V.; Huang, P.; Styring, S. *Dalton. Trans.* **2010**, *39*, 2344.

(8) (a) Boskovic, C.; Bircher, R.; Tregenna-Piggott, P. L. W.; Gudel, H. U.; Paulsen, C.; Wernsdorfer, W.; Barra, A.-L.; Khatsko, E.; Neels, A.; Stoeckli-Evans, H. *J. Am. Chem. Soc.* **2003**, *125*, 14046. (b) Oshio, H.; Hoshino, N.; Ito, T. *J. Am. Chem. Soc.* **2000**, *122*, 12602. (c) Oshio, H.; Hoshino, N.; Ito, T.; Nakano, M. *J. Am. Chem. Soc.* **2004**, *126*, 8805. (d) Li, Y.; Wu, Q.; Lecren, L.; Clerac, R. *J. Mol. Struct.* **2008**, *890*, 339.

(9) Spectral Database for Organic Compounds (SDBSWeb): http://riodb01.ibase.aist.go.jp/sdbs/; National Institute of Advanced Industrial Science and Technology (AIST), Japan.

(10) CSD (version 5.32; November 2011): Allen, F. H. *Acta Crystallogr.* **2002**, *B58*, 380.

(11) Nesterov, D. S.; Kokozay, V. N.; Skelton, B. W. *Eur. J. Inorg. Chem.* **2009**, 5469.

(12) Konno, T.; Tokuda, K.; Sakurai, J.; Okamoto, K. *Bull. Chem. Soc. Jpn.* **2000**, *73*, 2767.

(13) (a) Owen, J. *J. Appl. Phys.* **1961**, *32*, 213S. (b) Abragam, A.; Bleaney, B. In *Electron Spin Resonance of Transition Ions*; Clarendon Press: London, U.K., 1970. (c) Bencini, A.; Gatteschi, D. In *EPR of Exchange Coupled Systems*; Springer Verlag: Berlin, Germany, 1990. (d) Okamura, M. Y.; Hoffman, B. M. *J. Chem. Phys.* **1969**, *51*, 3128. (e) Ozarowski, A.; McGarvey, B. R.; Drake, J. E. *Inorg. Chem.* **1995**, *34*, 5558. (f) Chygorin, E. N.; Nesterova, O. V.; Rusanova, J. A.; Kokozay, V. N.; Bon, V. V.; Boca, R.; Ozarowski, A. *Inorg. Chem.* **2012**, *51* (1), 386. (g) Ozarowski A. et al., in preparation. (h) ter Heerdt, P.; Stefan, M.; Goovaerts, E.; Caneschi, A.; Cornia, A. *J. Magn. Reson.* **2006**, *179*, 29.

(14) Semenaka, V. V.; Nesterova, O. V.; Kokozay, V. N.; Dyakonenko, V. V.; Zubatyuk, R. I.; Shishkin, O. V.; Boca, R.; Jezierska, J.; Ozarowski, A. *Inorg. Chem.* **2010**, *49*, 5460.

(15) (a) Shul'pin, G. B. *J. Mol. Catal. A: Chem.* **2002**, *189*, 39. (b) Shul'pin, G. B. *C. R. Chim.* **2003**, *6*, 163. (c) Shul'pin, G. B. *Mini-Rev. Org. Chem.* **2009**, *6*, 95. (d) Shul'pin, G. B.; Kozlov, Y. N.; Shul'pina, L. S.; Kudinov, A. R.; Mandelli, D. *Inorg. Chem.* **2009**, *48*, 10480. (e) Shul'pin, G. B.; Kozlov, Y. N.; Shul'pina, L. S.; Petrovskiy, P. V. *Appl. Organomet. Chem.* **2010**, *24*, 464.

(16) See, for example: (a) Kirillov, A. M.; Kopylovich, M. N.; Kirillova, M. V.; Haukka, M.; da Silva, M. F. C. G.; Pombeiro, A. J. L. *Angew. Chem., Int. Ed.* **2005**, *44*, 4345. (b) Trettenhahn, G.; Nagl, M.; Neuwirth, N.; Arion, V. B.; Jary, W.; Pochlauer, P.; Schmid, W. *Angew. Chem., Int. Ed.* **2006**, *45*, 2794. (c) Di Nicola, C.; Garau, F.; Karabach, Y. Y.; Martins, L. M. D. R. S.; Monari, M.; Pandolfo, L.; Pettinari, C.; Pombeiro, A. J. L. *Eur. J. Inorg. Chem.* **2009**, 666. (d) Fernandes, R. R.; Lasri, J.; Kirillov, A. M.; da Silva, M. F. C. G.; da Silva, J. A. L.; da Silva, J. J. R. F.; Pombeiro, A. J. L. *Eur. J. Inorg. Chem.* **2011**, 3781. (e) Fernandes, R. R.; Lasri, J.; da Silva, M. F. C. G.; da Silva, J. A. L.; da Silva, J. J. R. F.; Pombeiro, A. J. L. *Appl. Catal., A* **2011**, *402*, 110.

(17) (a) Shul'pin, G. B. *Org. Biomol. Chem.* **2010**, *8*, 4217. (b) Nizova, G. V.; Krebs, B.; Süss-Fink, G.; Schindler, S.; Westerheide, L.; Gonzalez Cuervo, L.; Shul'pin, G. B. *Tetrahedron* **2002**, *58*, 9231. (c) Kirillova, M. V.; Kuznetsov, M. L.; Romakh, V. B.; Shul'pina, L. S.; Fraústo da Silva, J. J. R.; Pombeiro, A. J. L.; Shul'pin, G. B. *J. Catal.* **2009**, *267*, 140. (d) Shul'pina, L. S.; Kirillova, M. V.; Pombeiro, A. J. L.; Shul'pin, G. B. *Tetrahedron* **2009**, *65*, 2424. (e) Mandelli, D.; Chiacchio, K. C.; Kozlov, Y. N.; Shul'pin, G. B. *Tetrahedron Lett.* **2008**, *49*, 6693.

(18) (a) Süss-Fink, G.; Nizova, G. V.; Stanislas, S.; Shul'pin, G. B. *J. Mol. Catal. A: Chem.* **1998**, *130*, 163. (b) Shul'pin, G. B.; Nizova, G. V.; Kozlov, Y. N.; Gonzalez Cuervo, L.; Süss-Fink, G. *Adv. Synth. Catal.* **2004**, *346*, 317. (c) Kozlov, Y. N.; Nizova, G. V.; Shul'pin, G. B. *J. Mol. Catal. A: Chem.* **2005**, *227*, 247.

(19) (a) Shul'pin, G. B.; Kirillova, M. V.; Kozlov, Y. N.; Shul'pina, L. S.; Kudinov, A. R.; Pombeiro, A. J. L. *J. Catal.* **2011**, *277*, 164. (b) Shul'pin, G. B.; Kozlov, Y. N.; Nizova, G. V.; Süss-Fink, G.; Stanislas, S.; Kitaygorodskiy, A.; Kulikova, V. S. *J. Chem. Soc., Perkin Trans. 2* **2001**, 1351.

(20) (a) Mirza, S. A.; Bocquet, B.; Robyr, C.; Thomi, S.; Williams, A. F. *Inorg. Chem.* **1996**, *35*, 1332. (b) Rush, J. D.; Koppenol, W. H. *J. Am. Chem. Soc.* **1988**, *110*, 4957. (c) Bull, C.; McClune, G. J.; Fee, J. A. *J. Am. Chem. Soc.* **1983**, *105*, 5290. (d) Shinohara, N.; Matsufuji, S.; Okubo, W. *Polyhedron* **1991**, *10*, 107.

(21) (a) Fokin, A. A.; Schreiner, P. R. *Chem. Rev.* **2002**, *102*, 1551. (b) Newhouse, T.; Baran, P. S. *Angew. Chem., Int. Ed.* **2011**, *50*, 3362. (c) Buda, F.; Ensing, B.; Gribnau, M. C. M.; Baerends, E. J. *Chem.—Eur. J.* **2001**, *7*, 2775. (d) Gozzo, F. *J. Mol. Catal. A: Chem.* **2001**, *171*, 1.

(22) Shul'pin, G. B.; Golfeto, C. C.; Süss-Fink, G.; Shul'pina, L. S.; Mandelli, D. *Tetrahedron Lett.* **2005**, *46*, 4563.

(23) *SADABS, SAINT, SHELXTL and SMART*; Bruker AXS Inc.: Madison, WI, 2003.

(24) (a) Spek, A. L. *Acta Crystallogr.* **1990**, *A46*, C34. (b) Spek, A. L. *J. Appl. Crystallogr.* **2003**, *36*, 7. (c) Spek, A. L. *PLATON, A Multipurpose Crystallographic Tool*; Utrecht University: Utrecht, The Netherlands, 2000.

(25) Hassan, A. K.; Pardi, L. A.; Krzystek, J.; Sienkiewicz, A.; Goy, P.; Rohrer, M.; Brunel, L.-C. *J. Magn. Reson.* **2000**, *142*, 300.